An Ultra-broadband Polarization-Insensitive Optical Hybrid using Multiplane Light Conversion

Yuanhang Zhang, Nicolas K. Fontaine*, Haoshuo Chen, Roland Ryf, David T. Neilson, Joel Carpenter, and Guifang Li

Abstract—We designed, fabricated, and tested a 90 ° optical hybrid using multiplane light conversion. The device supports an octave of bandwidth (900 – 1800 nm) in simulations. The measured phase errors are below 3° for free space output, and below 8° with a fiber array output, across a measurement bandwidth of 390 nm. The fully-packaged device (with input and output fiber arrays) has a measured insertion loss of 5.52 dB at 1550 nm. A high-speed transmission experiment with QPSK format was conducted to verify the performance of the fully-packaged device.

Index Terms — optical hybrid, multiplane light conversion, mode multiplexer, broadband

I. INTRODUCTION

PTICAL hybrid [1] is well known as a key component in coherent receivers of optical communications. It can be constructed using various technologies including fiber, silicon photonics and using polarization optics [2-5]. Scaling the usable bandwidth to match the entire range of a photodetector could enable new applications, such as coherent spectroscopy [6], fiber sensing [7], light detection and ranging (LiDAR) [8], as well as biomedical sensing and imaging [9] such as optical coherence tomography (OCT) [10]. Among fabricated hybrids reported so far, the largest bandwidth is 120 nm around 1550 nm due to difficulties in obtaining an accurate 90° phase shift without active adjustments [11-13].

Multiplane light conversion (MPLC) is a multiple input, multiple output beam reshaping technique that consists of a series of phase masks separated by free space propagation [14, 15] and therefore could produce an optical hybrid which has 2 inputs and 4 outputs. Figure 1 shows the schematic of an optical hybrid formed in a multi-bounce cavity comprising 14 smooth phase masks and a gold mirror. The input is fed by a single mode fiber array collimated by micro-lenses, and the outputs are four Gaussian beams that are mode matched to a similar fiber collimator array or could be detected on free-space photodetectors.

Y. Zhang and G. Li are with CREOL, The College of Optics and Photonics, University of Central Florida, Orlando, FL 32816, USA (e-mail: yuanhangzhang@knights.ucf.edu li@creol.ucf.edu).

H. Chen, R. Ryf, D. T. Neilson, and N. K. Fontaine are with Nokia Bell Labs, Crawford Hill Lab, 791 Holmdel-Keyport Rd, Holmdel, NJ 07733, USA (e-mail: haoshuo.chen@nokia-bell-labs.com; <a href="mailto:rolland:rollan

Recently, different devices based on the principle of MPLC have been proposed. A mode sorter that is capable of largescale, two-dimensional spatial decomposition in the Laguerre Gaussian mode basis was demonstrated [16, 17]. A waveguideto-fiber mode coupler was designed to bridge few-mode fibers (FMF) and integrated optics in mode-division multiplexing (MDM) [18-20]. By incorporating the functionality of mode demultiplexing, local oscillator power splitting, and optical 90° mixing into one device, a mode demultiplexer hybrid (MDH) was proposed to significantly simplify the optical front end of mode-division multiplexing receivers [21]. With alternating phase modulation and dispersion, an optical arbitrary waveform generator based on time-domain MPLC was realized [22]. In paper, instead of exploring mode multiplexing/demultiplexing capability, we demonstrate the potential of building ultra-broadband devices use a large number of smooth phase masks. Our preliminary results for the MPLC-based ultra-broadband optical hybrid have been reported in [23]. Here we couple the free-space outputs to a collimated fiber array, making it a fully-packaged device and demonstrate its high performance in a high-speed coherent transmission experiment.

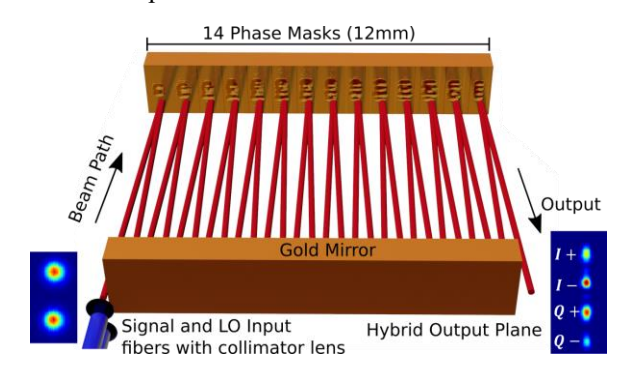


Fig.1 Schematic of the 90° optical hybrid using multiplane light conversion. The input beams come from a collimated fiber array. The output beams are designed to couple into a similar $250~\mu m$ pitch fiber array or a free space photodetector array using microlenses.

Joel Carpenter is with The University of Queensland, Brisbane, QLD 4027, Australia (e-mail: j.carpenter@uq.edu.au)

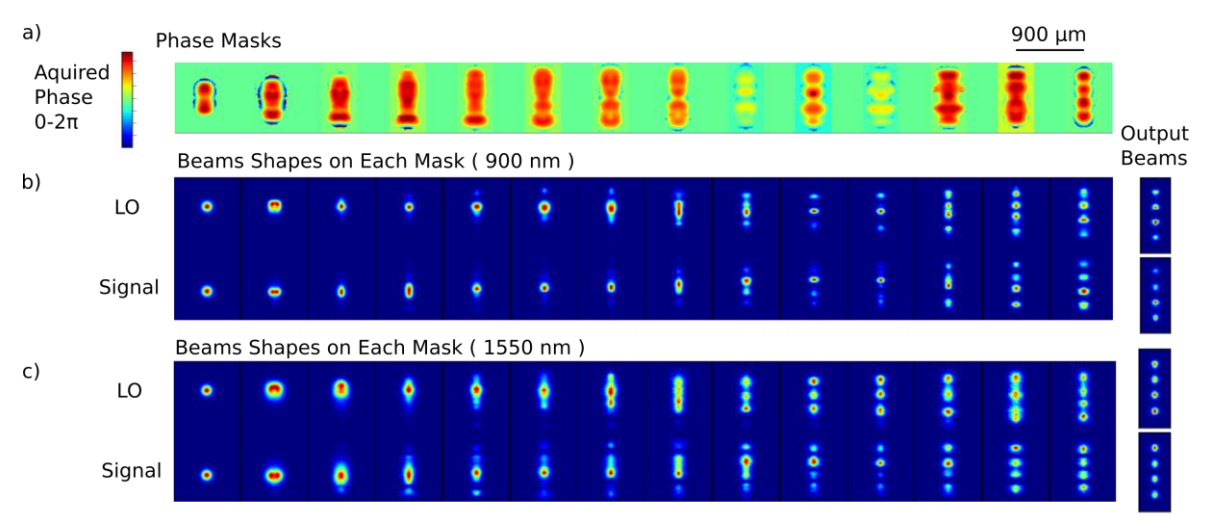


Fig. 2 Design and simulation of the hybrid at two different wavelengths (900 nm and 1550 nm) a) Phase masks, and beam shapes at each of the planes for b) 900 nm and c) 1550 nm input. Phase masks are relatively flat, lens like, smooth, and have no phase wraps.

MPLC based ultra-broadband devices have numerous advantages over waveguides and other free-space technologies. Primarily, ultra-broadband operation can be achieved because most of the light just propagates without loss in free space with very gentle phase modifications by reflective phase masks. In particular, it is in principle possible to produce devices operating in the mid infrared or in the ultraviolet if desired, where waveguides would typically have high losses or require exotic materials. Additionally, the technology to fabricate phase masks is mature, which has the potential for large scale production with low cost.

This paper is structured as follows. Section II describes the design principle and simulation of the MPLC optical hybrid. Section III briefly shows the fabrication and assembling of the device. Section IV presents the device characterization results (phase error and imbalance) with output in free space, and through a collimated fiber array. Results of a high-speed QPSK transmission experiment was shown in section V. Section VI compares our work with other published broadband hybrids and shows our design is tolerant to temperature changes. Finally, section VII summarizes this work.

II. DESIGN AND SIMULATION

An optical hybrid can be described as a unitary transformation of two spatial modes [21]. The two input modes, the local oscillator (LO) and the signal, are spatially separated Gaussian beams and hence orthogonal. The two output modes are a composite of 4 equally spaced Gaussian beams with identical power but different phases. In a 90-degree optical hybrid, the two output modes are also orthogonal because the phase differences between the beams generated from the LO and beams generated from the signal are 0, 180, 90, and 270 degrees, respectively.

In the MPLC hybrid design presented below, the plane spacing is set at 20 mm (10 mm mask-to-mirror distance) and the masks are separated horizontally by 900 μm. The design process uses inverse design techniques [24], specifically a

modified version of the wavefront matching algorithm [25], to optimize modes and corresponding phases over a broad range of wavelengths. For the detailed algorithm, the readers can refer to [16, 26].

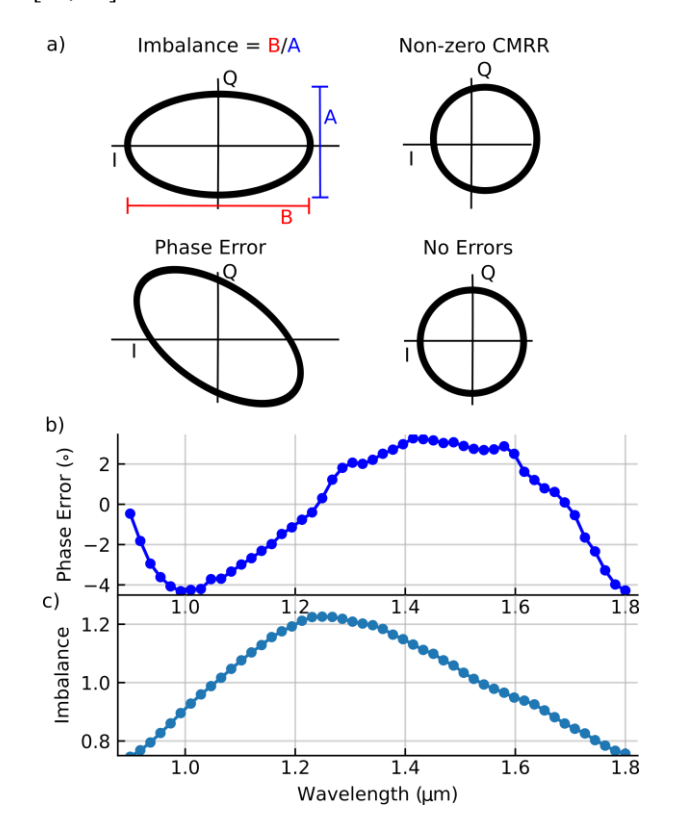


Fig. 3 Simulated performance of the MPLC hybrid. a) Constellations traced by an optical hybrid when two single frequency lasers are input to the LO and signal ports. Pure imbalance squishes the circle along I/Q axis, pure phase error skews the circle along 45° or 135° direction, and pure non-zero CMRR shifts away the center of the circle. Simulated hybrid b) phase error and c) imbalance across one octave of bandwidth (900 nm to 1800 nm).

Figure 2 shows the design and simulation of the hybrid. Based on simulations, 5 phase masks are sufficient to form an optical hybrid with a maximum 5° phase error over the C band (1530 nm - 1565 nm). However, when the number of phase masks is increased, the additional degrees of freedom provided can be used to significantly extend the bandwidth rather than to increase the number of supported modes [21]. Our broadband device uses 14 very smooth phase masks supporting an octave of bandwidth (900 -1800 nm) operation. Each mask imparts much less than π phase across the beams, has no phase wraps and looks similar to weak distorted lens. It should be noted that a smooth profile alone does not ensure wavelength independence since the phase shift provided by the relief structure changes by a factor of two across an octave of bandwidth. Figures 2 b) and c) show the beam intensity on each phase mask at 900 nm and 1550 nm. The beams slowly transit from a single spot to 4 equally spaced spots at the output plane. The shorter wavelength tends to be confined to smaller areas on most of the phase masks than the longer wavelength. Because the beams at different wavelengths are distributed differently across the mask, they will experience different phase modulations at each plane which can partially explain how the bandwidth can be increased.

Figure 3a) shows constellation plots when two equalintensity laser sources with random phase difference are input into the LO and signal ports. We choose to present the constellations because they show all imperfects a hybrid can have. A perfect hybrid traces a circle, a hybrid with pure phase error traces a tilted ellipse along 45° or 135° direction, a hybrid with only imbalance (different powers in I and Q arm) traces an ellipse aligned to the I/Q axis, and a hybrid with non-zero common mode rejection ratio (CMRR) will not be centered. To characterize the hybrid, we extract the imbalance and the phase error from the constellation. The CMRR of a hybrid can be compensated by simply adjusting the bias voltage of the balanced photodetector and is not considered here. Fig. 3 b) and c) show simulation of the hybrid across the full octave bandwidth, showing phase error below 5° and imbalance between 0.8 and 1.2.

III. FABRICATION AND ASSEMBLING

The phase masks were fabricated on a fused silica wafer using binary lithography method, which includes 6 subsequent steps of binary mask patterning and etching, giving 64 phase levels between 0 and 2π , corresponding to a etch depth between 0 and 775 nm. The pixel size of the phase mask was $5 \,\mu\text{m} \times 5 \,\mu\text{m}$. The mask was coated with gold to minimize absorption loss. A plane gold mirror was aligned 10 mm away to fold the beam and allow multiple bounces on the phase masks. The input came from two adjacent fibers from a collimated fiber array, which has a 250 µm pitch and 70 µm beam waist. The incident angle of the beam is 2.57°. The four output beams were coupled into a similar collimated fiber array. The input and output fiber arrays were placed 15 mm from the first and last phase masks, respectively. Picture of the assembled device is shown in Fig. 4. The gold mirror, input and output fiber arrays were held by three six-axis stages (x, y, z, pitch, yaw and roll) in the assembling process for easy

optimization, while the phase plane was glued on a stage in advance. Once the performance was optimized, we used glass blocks and UV curing epoxy to secure the fiber arrays and gold mirror in place.

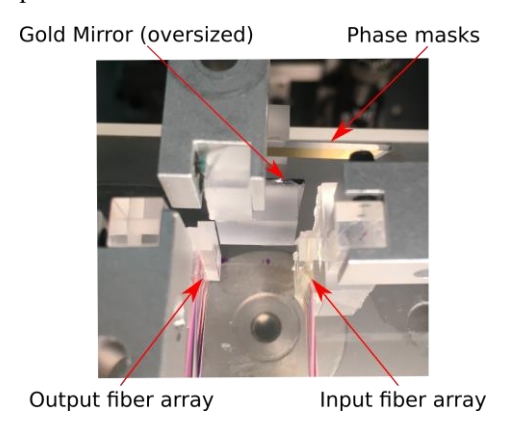


Fig. 4 Photograph of the assembled MPLC hybrid. Once the performance was optimized, we used glass blocks and UV curing epoxy to secure the fiber arrays and the mirror in place.

IV. DEVICE CHARACTERIZATION

The performance of the hybrid was optimized in free-space first before coupling into the output fiber array. Coherent light from a tunable laser was split into two with equal power, feeding the two input ports of the MPLC hybrid. After the 50:50 fiber coupler, one arm was delayed by a 20-m long fiber delay line so that the random frequency drift of the laser will accumulate enough phase changes on the I-Q complex plane. At the exit port of the hybrid, an imaging lens (shown in a dashed box in Fig. 5) with a focal length of 100 mm was used to image the output beam onto an InGaAs camera.

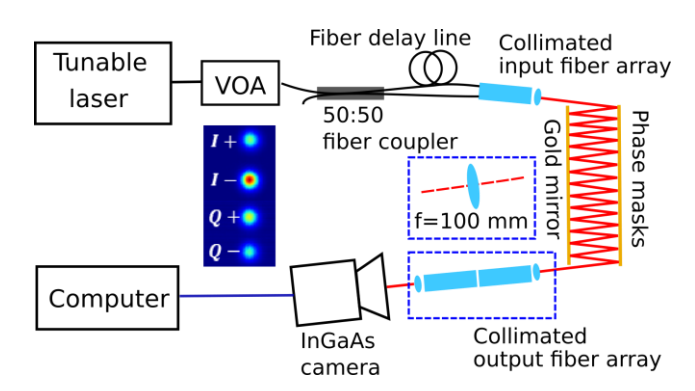


Fig. 5 Experimental setup to optimize the device performance before (with a lens in the dashed box) and after (with a pair of fiber arrays in the dashed box) coupling the output beam into the output fiber array. Red lines indicate beams in free space. The inset photo shows four output beam spots on the camera after coupling into the output fiber array. VOA: variable optical attenuator.

Measurements were conducted between 1260 nm and 1650 nm due to the limitation of available light sources. Two tunable external cavity lasers were used, one in the O-band and one in the S+C+L-band. The output polarizations were split by a Wollaston prism after the lens and 8 spots were measured on an InGaAs camera. For each image, one constellation value for each polarization could be calculated from the intensity of the 8 spots (2 polarizations). 2000 images were taken at each

wavelength to acquire enough data to produce a constellation. The phase errors were calculated by curve fitting to the measured constellation.

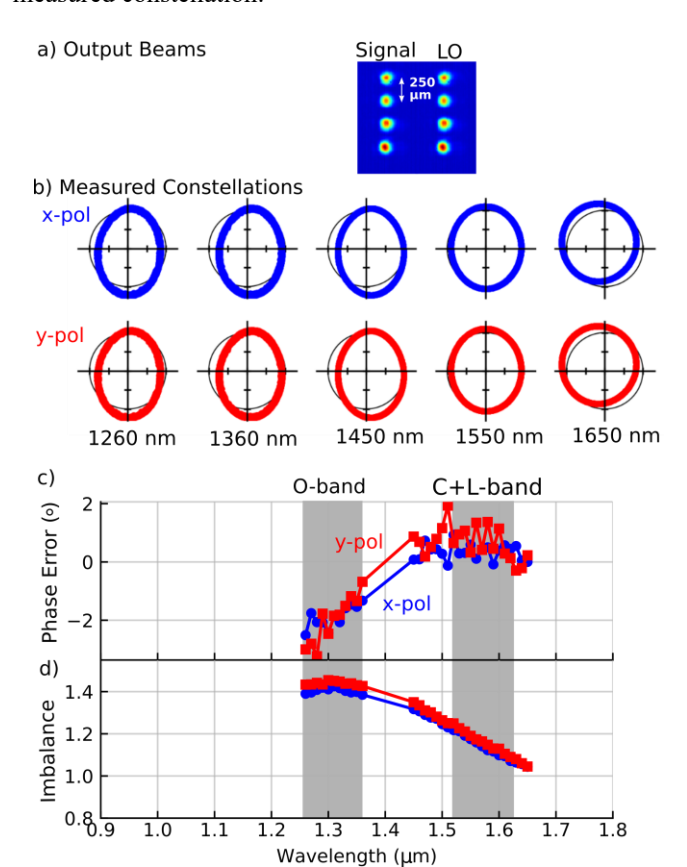


Fig. 6 Measured performance of hybrid between 1260 nm and 1650 nm. a) Output beams when launching light in only the LO or signal ports, showing spatial profiles with spacing of 250 μm . b) Measured constellations for the two polarizations at five wavelengths. Ideal constellation indicated as a black circle. c) Phase error across the measurement range (1260 nm - 1650 nm) is below $\pm 3^{\circ}$. Markers indicates measurement points. d) Measured imbalance at different wavelengths.

Figure 6 a) shows that the measured output beams in free space when launching light in only the LO or Signal ports, showing Gaussian-shaped spatial profiles with spacing of 250 µm. Figure 6 b) shows the constellations at the different wavelengths, in comparison with the ideal constellation (i.e., unit circle). Figures. 6 c) and d) plot the curve fitted results for hybrid phase error and imbalance. Towards the shorter wavelengths, there are slight phase errors in the hybrid that skews the constellation. The imbalance of this hybrid is much larger than the phase error, however, imbalance is typically fixed by adjusting the gains of the photodetectors whereas phase error cannot be compensated as simply. X- and y-polarization curves in c) and d) almost overlap, indicating our device is almost polarization insensitive.

Once the device performance was optimized, we would fix the positions of the input fiber array and the gold mirror, and then couple the output into a second collimated fiber array. To observe the image on the InGaAs camera this time, we connected another collimated fiber array to the second 250-µm fiber array, i.e., using a pair of fiber arrays instead of a single lens (indicated by dashed blue boxes in Fig. 5) to image on the camera. With the fully packaged device (with the output fiber array), we did not verify its polarization dependence.

Four adjacent ports were used in the output fiber array, where the pair of I+ and I-, Q+ and Q- were length matched respectively to align the signal pulse in time domain. The length of each arm was measured to a precision of 0.1 ps using an optical vector network analyzer (OVNA) [27, 28]. Two tunable optical fiber delay lines (Santec, 330 ps range) were inserted into the I+ and Q+ arm to match that length of I- and Q- arm, respectively. Length (delay) of I+ and I- arms are matched to be 21.1156 ns, while length (delay) of Q+ and Q- arms are matched to be 20.8328 ns. I and Q are not matched due to limited number of fiber delay lines.

The measured insertion loss of this fully packaged MPLC hybrid was 5.52 dB, which is reasonable considering the theoretical 2.37 dB of absorption by 27 reflections on the phase mask and gold mirror.

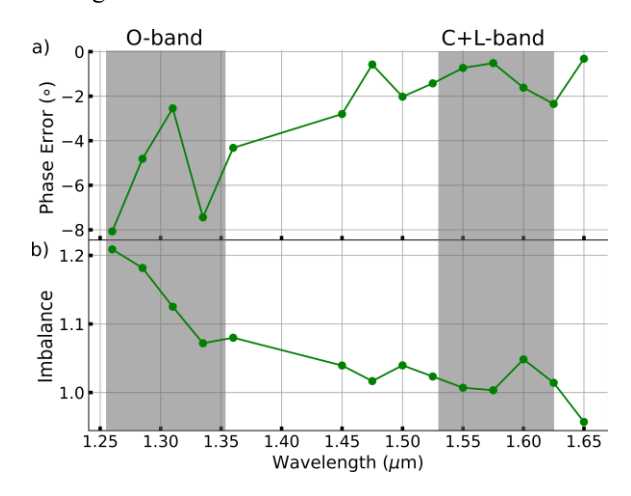


Fig. 7 Measured phase error and imbalance of the fully packaged hybrid.

Measurements for the fully-package hybrid is shown in Fig. 7. The phase error is between $-8^{\circ} \sim 0^{\circ}$, and the imbalance is between $0.95 \sim 1.2$. This phase errors for the fully-packaged hybrid is worse than those in Fig. 6 c) due to differences in lengths and coupling efficiencies of fibers in the output fiber array.

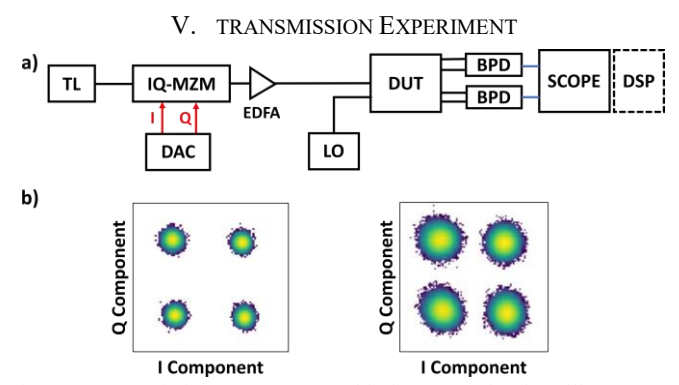


Fig. 8 a) Transmission setup. TL: tunable laser, LO: local oscillator, DUT: device under test, BPD: balanced photo detector, IQ-MZM: IQ Mach-Zehnder modulator. b) Recovered QPSK constellation for 30-Gbaud (left) and 60-Gbaud (right) signal, respectively.

T	ABLE I
PERFORMANCE COMPARISON O	OF BROADBAND 90° OPTICAL HYBRID

Year	Ref	Phase error	Bandwidth	Structure*	
2010	[3]	Φ < 5°	94 nm	A 2×4 MMI coupler, a phase shifter, and a 2×2 MMI coupler	Experiment
2011	[11]	Φ < 3°	~ 120 nm	Highly symmetrical interferometer design	Experiment
2018	[12]	Φ < 5°	~ 150 nm	Inter-polarization electro-magnetic mixer	Simulation
2018	[29]	Φ < 5°	156 nm	Subwavelength grating dispersion-engineered 2×4 MMI coupler	Simulation
2020	This work	Φ < 3°	390 nm	Free-space multiplane light conversion	Experiment

^{*}MMI: multimode interference

A back-to-back transmission experiment was conducted to verify the performance of the fully packaged device, as shown in Fig. 8 a). A stable CW laser at 1550.143nm was used as the local oscillator. The tunable laser, also fixed at 1550.143nm, was modulated with a 30-Gbaud or a 60-Gbaud quadrature phase shift keying (QPSK) signal using an IQ Mach-Zehnder modulator (IQ-MZM), respectively. The IQ-MZM was driven by a 2-channel programmable digital-to-analog converter (DAC). One inline EDFA was used to amplify the optical signal after the modulator. At the output of the MPLC hybrid, the four length-matched ports were connected to two balanced photo detectors (BPD), and the electrical waveforms at the outputs of the BPDs were captured by a real-time oscilloscope (KEYSIGHT DSOZ634A) at a sampling rate of 160 GSamples/s. All data were collected and processed by offline digital signal processing (DSP) afterwards. The recovered QPSK constellations are shown in Fig. 8 b), demonstrating the functionality of the MPLC hybrid.

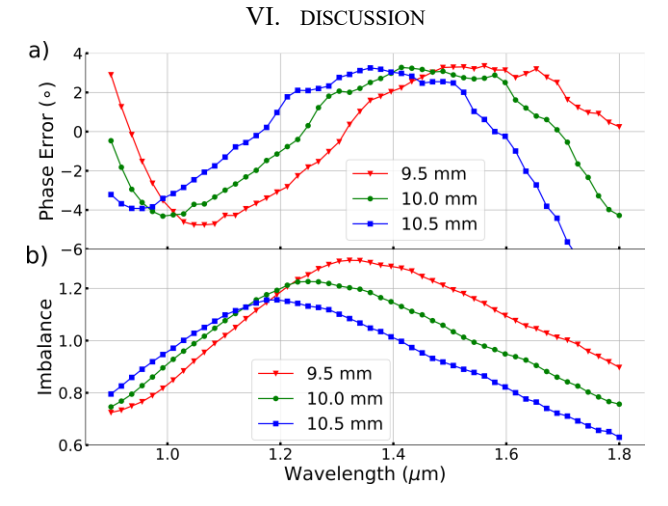


Fig. 9 Simulated performance of the hybrid at different mask-mirror spacings. a) Phase error curve shifts horizontally to shorter wavelength as the spacing increases. And the b) imbalance curve shifts down-left as the spacing increases.

In TABLE I we compare some major metrics of our work with published works on broadband 90° hybrids.

The UV epoxy we used (Dymax, OP-4-20632) to glue the glass blocks changes from a rubbery elastic phase to a rigid crystalline phase after curing, which has a low coefficient of thermal expansion (CTE $\alpha_1 = 54~\mu$ m/m/ $^{\circ}$ C) [30]. To demonstrate this hybrid is tolerant to temperature changes, we simulate performance of the hybrid as the mask-mirror spacing deviates $\pm 500~\mu m$ from the designed 10 mm. Fig. 9 shows that both phase error curve and imbalance curve shift horizontally to shorter wavelength as the mask-mirror spacing increases, while the imbalance curve has an extra shift in the downward direction.

VII. CONCLUSION

In conclusion, we successfully demonstrated the idea of building a ultrabroad bandwidth optical 90° hybrid using the multiplane light conversion technique. The measured phase errors are below 3° for free space output and below 8° for fiber array output, across a measurement bandwidth of 390 nm. The measured insertion loss of a fully packaged device is 5.52 dB. Simulation shows this device is tolerant to temperature changes.

ACKNOWLEDGMENT

The authors would like to thank Xi Chen and Di Che in Nokia Bell Labs for the oscilloscope and tunable fiber delay lines. Yuanhang Zhang acknowledges the financial support from the China Scholarship Council (CSC) Scholarship No. 201606250006.

REFERENCES

- [1] Leeb, W. "Realization of 900 and 180 hybrids for optical frequencies." *Electron. Commun.* AEU 37 (1983).
- [2] Seimetz, Matthias, and C-M. Weinert. "Options, feasibility, and availability of 2×4 90° hybrids for coherent optical systems." *J. Lightw. Technol.*, 24.3 (2006): 1317-1322.
- [3] Jeong, Seok-Hwan, and Ken Morito. "Novel Optical 90° Hybrid Consisting of a Paired Interference Based 2×4 MMI Coupler, a Phase Shifter and a 2×2 MMI Coupler." *J. Lightw. Technol.*, 28.9 (2010): 1323-1331.
- [4] Jeong, Seok-Hwan, and Ken Morito. "Optical 45° hybrid for demodulating 8-ary DPSK signal." *Opt. Express*, 18.8 (2010): 8482-8490.

6

> REPLACE THIS LINE WITH YOUR PAPER IDENTIFICATION NUMBER (DOUBLE-CLICK HERE TO EDIT) <

- [5] Doerr, Christopher R. et al. "Monolithic InP multiwavelength coherent receiver using a chirped arrayed waveguide grating." *J. Lightw. Technol.*, 29.4 (2011): 536-541.
- [6] Hashimoto, Kazuki, et al. "Broadband coherent Raman spectroscopy running at 24,000 spectra per second." Sci. Rep., 6 (2016): 21036.
- [7] Haran, Frank Martin, Ross MacHattie, and Ronald E. Beselt. "Fiber optic sensor utilizing broadband sources." *U.S. Patent* No. 8,085,397. 27 Dec. 2011.
- [8] Romanovskii, Oleg A., et al. "Broadband IR lidar for gas analysis of the atmosphere." J. Appl. Spectrosc., 85.3 (2018): 457-461.
- [9] Yan, Di, et al. "Highly sensitive broadband Raman sensing of antibiotics in step-index hollow-core photonic crystal fibers." ACS Photonics, 4.1 (2017): 138-145.
- [10] Winkelmann, James A., *et al.* "In vivo broadband visible light optical coherence tomography probe enables inverse spectroscopic analysis." *Opt. Lett.*, 43.3 (2018): 619-622.
- [11] Nasu, Yusuke, *et al.* "Temperature insensitive and ultra-wideband silicabased dual polarization optical hybrid for coherent receiver with highly symmetrical interferometer design." *Opt. Express*, 19.26 (2011): B112-B118.
- [12] Melikyan, Argishti, *et al.* "Inter-polarization mixers for coherent detection of optical signals." *Opt. Express*, 26.14 (2018): 18523-18531.
- [13] Xu, Luhua, *et al.* "Compact high-performance adiabatic 3-dB coupler enabled by subwavelength grating slot in the silicon-on-insulator platform." *Opt. Express*, 26.23 (2018): 29873-29885.
- [14] Morizur, Jean-François, et al. "Programmable unitary spatial mode manipulation." J. Opt. Soc. Am. A, 27.11 (2010): 2524-2531.
- [15] Labroille, Guillaume, *et al.* "Efficient and mode-selective spatial mode multiplexer based on multi-plane light conversion." *Opt. Express*, 22.13 (2014): 15599-15607.
- [16] Fontaine, Nicolas K., et al. Laguerre-Gaussian mode sorter. Nat. Commun., 10, 1865 (2019): 1-7.
- [17] Fontaine, Nicolas K., et al. "Laguerre-Gaussian mode sorters of high spatial mode count." Advances in Optical Astronomical Instrumentation 2019. Vol. 11203. International Society for Optics and Photonics, 2020.
- [18] Zhang, Yuanhang, *et al.* "Slab Waveguide-to-Fiber Coupling based on Multiplane Light Conversion." *Frontiers in Optics.* pp. FW1B-3. Optical Society of America, 2019.
- [19] Li, Chenlei, Dajian Liu, and Daoxin Dai. "Multimode silicon photonics." *Nanophotonics*, 8.2 (2018): 227-247.
- [20] Zhang, Yuanhang, et al. "An Integrated Few-Mode Power Splitter Based on Multimode Interference." J. Lightw. Technol., 37.13 (2019): 3000-3008.
- [21] Wen, He, et al. "Mode demultiplexing hybrids for mode-division multiplexing coherent receivers." *Photonics Res.*, 7.8 (2019): 917-925.
- [22] Mazur, Mikael, et al. "Optical Arbitrary Waveform Generator Based on Time-Domain Multiplane Light Conversion." 2019 Optical Fiber Communications Conference (OFC). pp.1-3.
- [23] Fontaine, N. K. *et al.* "Ultrabroadband Polarization Insensitive Hybrid using Multiplane Light Conversion", 2020 *Optical Fiber Communication Conference (OFC)*, paper W4C.5.
- [24] Lalau-Keraly, Christopher M., et al. "Adjoint shape optimization applied to electromagnetic design." Opt. Express, 21.18 (2013): 21693-21701.
- [25] Hashimoto, T., et al. "Optical circuit design based on a wavefront-matching method." Opt. Lett. 30.19 (2005): 2620-2622.
- [26] Fontaine, Nicolas K., et al. "Design of high order mode-multiplexers using multiplane light conversion." 2017 European Conference on Optical Communication (ECOC). pp. 1-3.
- [27] Fontaine, Nicolas K., et al. "Characterization of space-division multiplexing systems using a swept-wavelength interferometer." 2013 Optical Fiber Communication Conference. pp. OW1K-2.
- [28] VanWiggeren, Gregory D., and Douglas M. Baney. "Swept-wavelength interferometric analysis of multiport components." *IEEE Photon. Techno. Lett.* 15.9 (2003): 1267-1269.
- [29] Xu, Luhua, *et al.* "Ultra-broadband and ultra-compact optical 90° hybrid based on 2×4 MMI coupler with subwavelength gratings on silicon-on-insulator." *2018 Optical Fiber Communication Conference (OFC)*. pp. M3I-7. [30] https://www.dymax.com/images/pdf/pds/op-4-20632.pdf